Check for updates

CHEMISTRY
A European Journal

A Journal of
ChemPubSoc Europe

Accepted Article

Title: Competitive metal-coordination of hexaaminotriphenylene on Cu(111) by intrinsic copper versus extrinsic nickel adatoms

Authors: Matthias Lischka, Renhao Dong, Mingchao Wang, Natalia Martsinovich, Massimo Fritton, Lukas Grossmann, Wolfgang M Heckl, Xinliang Feng, and Markus Lackinger

This manuscript has been accepted after peer review and appears as an Accepted Article online prior to editing, proofing, and formal publication of the final Version of Record (VoR). This work is currently citable by using the Digital Object Identifier (DOI) given below. The VoR will be published online in Early View as soon as possible and may be different to this Accepted Article as a result of editing. Readers should obtain the VoR from the journal website shown below when it is published to ensure accuracy of information. The authors are responsible for the content of this Accepted Article.

To be cited as: *Chem. Eur. J.* 10.1002/chem.201803908

Link to VoR: http://dx.doi.org/10.1002/chem.201803908

Supported by
ACES

WILEY-VCH

10.1002/chem.201803908

WILEY-VCH

Competitive metal-coordination of hexaaminotriphenylene on Cu(111) by intrinsic copper *versus* extrinsic nickel adatoms

Matthias Lischka,[a],[b] Renhao Dong,[c] Mingchao Wang,[c] Natalia Martsinovich,[d] Massimo Fritton,[a],[b] Lukas Grossmann,[a],[b] Wolfgang M. Heckl,[a],[b],[e] Xinliang Feng,[c] and Markus Lackinger[a],[b],[e],*

Abstract: The interplay between self-assembly and surface chemistry of 2,3,6,7,10,11-hexaaminotriphenylene (HATP) on Cu(111) was complementarily studied by high-resolution Scanning-Tunneling-Microscopy (STM) and X-ray Photoelectron Spectroscopy (XPS) under ultra-high vacuum conditions. To shed light on competitive metal-coordination, comparative experiments were carried out on pristine and nickel-covered Cu(111). Directly after room temperature deposition of HATP onto pristine Cu(111) self-assembled aggregates were observed by STM, while XPS indicated non-deprotonated amino groups. Annealing up to 200 °C activated the progressive single deprotonation of all amino groups as indicated by chemical shifts of both N 1s and C 1s core levels in the XP spectra. This enabled the formation of topologically diverse π-d conjugated coordination networks with intrinsic copper adatoms. The basic motif of these networks was a metal-organic trimer, where three HATP molecules were coordinated by Cu_3 clusters, as corroborated by accompanying Density Functional Theory (DFT) simulations. Additional deposition of more reactive nickel atoms resulted in both chemical and structural changes with deprotonation and formation of bis(diimino)-Ni bonded networks already at room temperature. Even though fused hexagonal metal-coordinated pores were observed, extended honeycomb networks remained elusive, as tentatively explained by a restricted reversibility of these metal-organic bonds.

Introduction

The bottom-up synthesis of two-dimensional (2D) materials with regular structures and tailored properties is a long-standing goal in chemistry and material science.[1] A pivotal milestone was the materialization of 2D coordination nanosheets (CONASH), where multi-topic organic ligands are cross-linked into regular networks by metal-coordination bonds. The synthesis of square-centimeter large self-supporting sheets was pioneered at the air-water interface, and has subsequently also been demonstrated at the interface between two immiscible liquids.[2] For the latter, typically multilayers are achieved. For these interface-assisted synthetic approaches triphenylene-based organic ligands with six-fold hydroxyl, thiol, or amino functionalization at the 2,3,6,7,10,11 positions evolved as important model system.[3] The targeted binding motif is a planar four-fold coordination complex, and incorporation of Cu, Ni, and Co coordination centers yielded isostructural *π-d* conjugated CONASHs with honeycomb structure and widely tunable properties.[4] Superior electrical conductivities up to 10^3 S cm^{-1} were demonstrated, facilitating a variety of applications as electrode materials for organic field-effect transistor, chemiresistive sensing,[5] electrocatalytic hydrogen evolution reaction as well as oxygen reduction,[3a, 6] and supercapacitors.[3c, 3d, 7]

Despite the tremendous progress in the interface-assisted synthesis of large area CONASH, a molecular level structural characterization by high-resolution microscopy remains challenging. Even though recent advances were achieved for single-layer CONASH with high-resolution transmission electron microscopy,[8] the high electron beam sensitivity of these materials imposes severe limitations. On the contrary, submolecular features are routinely resolved by Scanning Tunneling Microcopy (STM) both on metal-coordination and covalent networks with minimal risk of sample damage. Yet, for networks grown at liquid interfaces, STM characterization requires a post-synthetic transfer to suitable solid surfaces, with only a few reported cases of successful imaging.[9] The reasons for the difficulties in *ex-situ* imaging of these networks are not entirely clear, but might be related to an unavoidable waviness after their transfer to solid surfaces, crucially impairing high resolution STM imaging. In contrast, both metal-coordination and covalent networks that were directly grown on solid surfaces under ultra-high vacuum (UHV) or even under ambient conditions are routinely imaged with high resolution.[10] Albeit requiring ultra-high vacuum (UHV) is not desirable in terms of a low-cost fabrication, fundamental studies can benefit greatly from these utmost defined conditions. For instance, a thorough chemical characterization by X-ray Photoelectron Spectroscopy (XPS) of *in-situ* prepared samples is not affected by contaminations that are unavoidable under ambient conditions. In the present study we focus on 2,3,6,7,10,11-hexaaminotriphenylene (HATP, cf. Fig. 1a). Despite the large body of work on nitrogen-containing metal-coordination networks with amines,[11] nitriles,[12] pyridines,[13] or amino-quinone-imines,[14] HATP or other ligands with *ortho*-disubstituted amino groups have not been investigated on solid surfaces so far. The only example of a related compound intended the on-surface synthesis of pyrene-fused pyrazaacenes *via* Schiff-base reaction.[15] To shed more light on the metal-coordination of this

[a] M. Lischka, M. Fritton, L. Grossmann, Prof. Dr. W.M. Heckl, Prof. Dr. M. Lackinger
Department of Physics, Technische Universität München
James-Franck-Str. 1, 85748 Garching, Germany
E-mail: markus@lackinger.org
[b] Center for NanoScience (CeNS) and Nanosystems-Initiative-Munich (NIM), Schellingstr. 4, 80799 München, Germany
[c] Dr. R. Dong, M. Wang, Prof. Dr. X. Feng
Center for Advancing Electronics Dresden (cfaed) and Department of Chemistry and Food Chemistry, Technische Universität Dresden, Mommsenstr. 4, 01069 Dresden, Germany
[d] Dr. N. Martsinovich
Department of Chemistry, University of Sheffield,
Sheffield, S3 7HF, UK
[e] Deutsches Museum, Museumsinsel 1, 80538 München, Germany
Supporting information for this article is given via a link at the end of the document.

Accepted Manuscript

This article is protected by copyright. All rights reserved.

important molecular building block on solid surfaces, we present a detailed study of competitive HATP metal-coordination on Cu(111) between intrinsic Cu adatoms of the surface[11, 14a] and co-deposited extrinsic Ni adatoms. This choice is motivated by a strong interest in comparing coordination centers with different binding strength and ground state electron configurations. The utilized combination of STM, XPS, and DFT provides the base for drawing solid and important conclusions on the interplay between surface chemistry and structure formation.

Results and Discussion

HATP on pristine Cu(111)

First experiments were conducted on pristine Cu(111). The STM images in Figure 1b and c acquired directly after room temperate deposition of HATP reveal self-assembled molecular aggregates. Cyclic hexamers are most abundant, but incomplete and fused hexamers as well as more densely packed structures were similarly observed. Individual HATP molecules and their respective orientation can be discerned by means of the triangular footprints of the planar adsorbed triphenylene cores. In the hexamers all HATP molecules point toward the center and share edges that are not fully aligned, but slightly offset. To unveil the stabilizing intermolecular bonds in these hexamers, acquiring complementary information on the chemical state of HATP is indispensable. In this respect, it is important to address the question of a possible deprotonation and formation of metal-coordination bonds of the amino groups already after room temperature deposition onto Cu(111).[11, 16] Therefore, XP spectra were acquired from N 1s and C 1s core levels, whereby the spectra of 3 - 4 layer thick films shown in Figures 2a and b served as references for chemically unaltered HATP molecules. The sharp N 1s peak indicates a single chemical species, corroborating the anticipated chemical equivalency of all nitrogen atoms. The measured binding energy (BE) of 399.8 eV is in accord with NH_2 groups on aromatic moieties, with similar BEs reported for aniline,[17] 1,3-phenyldiamine,[18] tetraamine,[15] and melamine[19] adsorbed on various metals surfaces. The C 1s XP spectrum shown in Figure 2b required fitting with two chemically shifted components with BEs of 284.7eV and 285.7 eV, resulting in a peak area ratio of 67:33. The C 1s component at higher BE corresponds to the amino-substituted carbons, the component at lower BE corresponds to the unsubstituted carbons of the triphenylene core.[17a, 20] Hence, the deduced ratio perfectly reflects the HATP stoichiometry.
The submonolayer spectra presented in Figures 2c and d are essentially similar to the multilayer. Only N 1s exhibits a slight shift of ~0.39 eV towards higher BE. Yet, core-hole screening and deprotonation would both result in shifts to lower BE, and can hence be excluded.[14, 17a, 19, 21] There are no notable shifts in C 1s, indicating a specific surface-influence on the nitrogen atoms, such as for instance formation of N-Cu bonds. In summary, XPS indicates adsorption of HATP molecules with intact NH_2 groups after room temperature deposition onto Cu(111), in accord with results obtained for a comparable

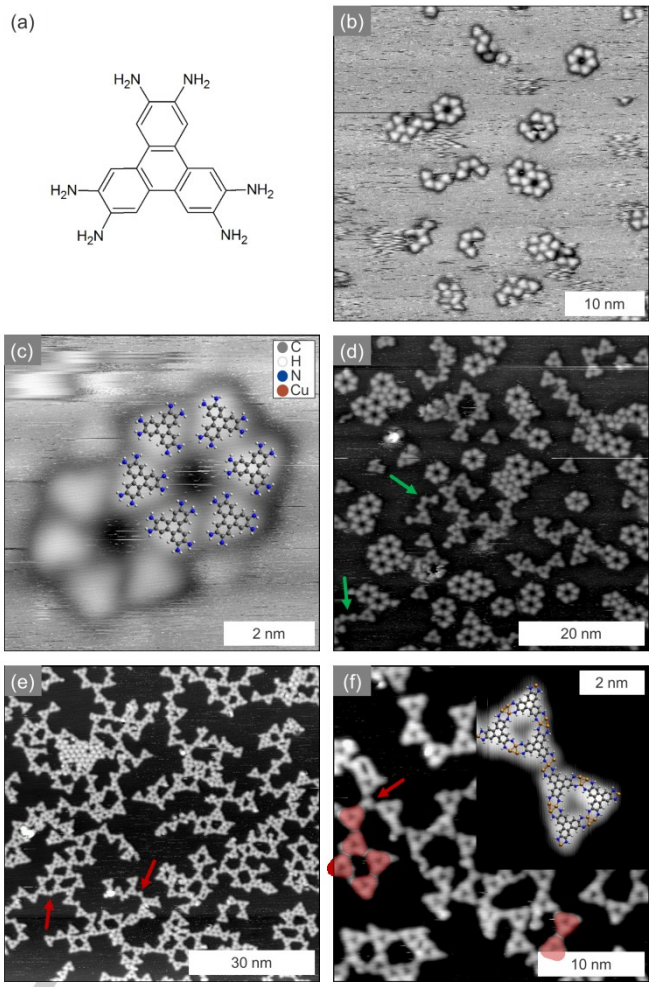

Figure 1. a) chemical structure of HATP; STM images acquired after b) / c) room temperature deposition of HATP onto Cu(111), and after subsequent annealing to d) 100 °C and e) / f) 200 °C; DFT-optimized structures were used for the overlays. c) depicts a HATP decamer comprised of two fused cyclic hexamers; d) annealing to 100 °C results in a mixture of van-der-Waals bonded and metal-coordinated structures; e) overview over predominantly metal coordinated structures obtained after annealing to 200 °C. The close up in f) shows that kinked dimers of Cu_3-coordinated molecular trimers (examples highlighted in red) represent the most abundant motif. The insert shows a close up of such a kinked dimer overlaid by a structure with a metal-coordination interlink comprised of three copper atoms. Green arrows indicate straight dimers, red arrows highlight single HATP molecules that interlink supramolecular trimers. tunneling parameters: a) 0.73 V, 54 pA; b) 0.73 V, 51 pA; c) 0.89 V, 59 pA; d) 0.87 V, 90 pA; (d, inset) 0.33 V, 20 pA)

compound.[22] Based on these XPS results, the formation of intermolecular metal-coordination bonds after room temperature deposition can be ruled out.

To address the question as to what other interactions drive the self-assembly of these aggregates, first DFT simulations of single HATP molecules on Cu(111) were conducted. Various starting geometries consistently resulted in adsorption geometries, where the centers of all aromatic rings of the triphenylene backbone resided above three-fold hollow sites

Accepted Manuscript

This article is protected by copyright. All rights reserved.

(either fcc- or hcp-sites). Accordingly, half of the carbon atoms also resided on three-fold hollow sites, and the remaining carbon atoms on top-sites of the Cu(111) surface. This preferred adsorption geometry is well known for benzene on transition metals,[23] and the close match between the spacing of adjacent aromatic rings in triphenylene (0.250 nm) and the Cu(111) lattice parameter (0.255 nm) makes this adsorption geometry also favorable for the larger aromatic core of HATP. In the next step, several competing models for the cyclic hexamers comprised of non-deprotonated HATP molecules as suggested by XPS were calculated on Cu(111) by DFT. All optimized structures reproduced the experimentally found molecular arrangement and intermolecular distances within the experimental error (cf. Supporting Information).

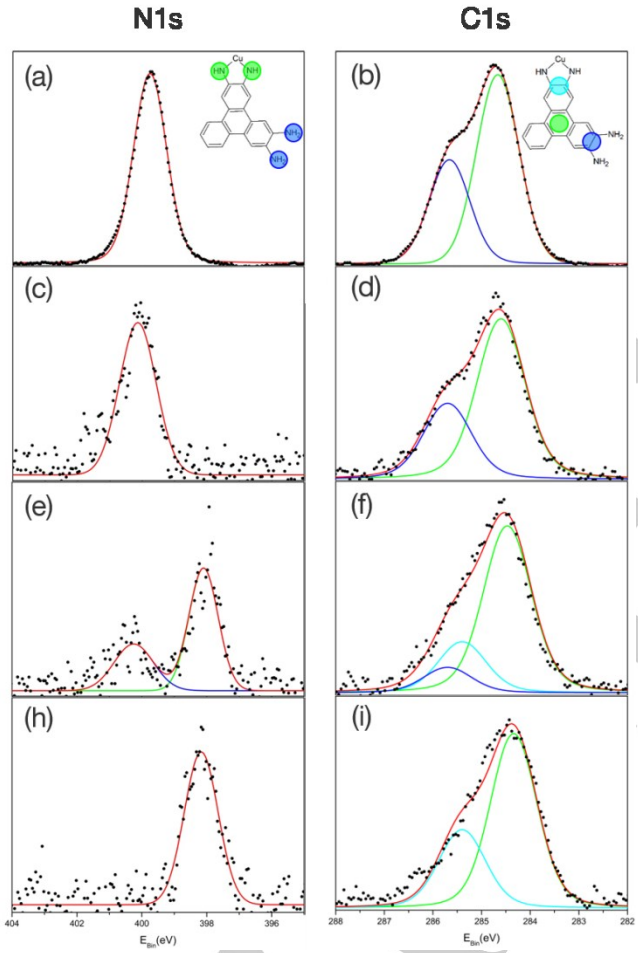

Figure 2. XP spectra of N 1s (left column) and C 1s (right column) acquired for HATP on Cu(111): a) / b) multilayer; c) / d) submonolayer after room temperature deposition and subsequent annealing to e) / f) 100 °C, and h) / i) 200 °C. Data are represented by black dots; red lines correspond to the sum of all fitted components; N 1s and C 1s components are assigned to the following colour scheme as also shown in the inset: NH_2 (green), NH-Cu (blue), C-C (green), C-NH_2 (blue), C-NH-Cu (light blue.)

Figure 3a exemplarily shows one structure, where all aromatic rings of all six HATP molecules reside above fcc-sites, which were consistently found to be 0.02 - 0.03 eV per molecule more favorable than hcp-sites. The mean adsorption height of HATP molecules in the hexamers (excluding H atoms) above the Cu(111) surface is (2.90 ± 0.09) Å, where the standard deviation was denoted as error bar. The hydrogen atoms point slightly down and are on average 2.72 Å above the surface. Extremely small adsorption height differences between fcc- and hcp-sites of around 0.01 Å provide further evidence for the equivalency of both adsorption geometries. The DFT-derived center-to-center distance of two diametrically opposed HATP molecules of 2.41 nm in the structure shown in Figure 3a (cf. Supporting Information) is in good agreement with the experimental value of (2.52 ± 0.06) nm. In the modelled hexamer structures half of the nitrogen atoms reside on top of copper atoms, additionally allowing N-Cu bond formation. While DFT indicates a rather strong adsorption of HATP on Cu(111) with adsorption energies around 4 eV per molecule, the intermolecular interactions in the hexamers are surprisingly weak, on the order of 0.06 - 0.18 eV per molecule. The disintegration of aggregates as tracked in subsequent STM images provides experimental evidence for a weak stabilization (cf. Supporting Information). Even though amino groups could in principle also act as hydrogen-bond acceptors through their nitrogen lone pair, the present DFT simulations do not provide any evidence for intermolecular hydrogen bonds. Since intermolecular metal-coordination and hydrogen bonds can be ruled out, we conclude that solely comparatively weak van-der-Waals interactions account for the cohesion of these aggregates, whereas the molecular orientation is determined by strong and highly site-specific molecule-surface interactions. It is worth noting that the variety of aggregates observed after room temperature deposition as illustrated in Figure 1b, as for instance fused cyclic hexamers (see Figure 1c), filled hexamers with an additional molecule inside the central pore, incomplete hexamers, or more densely packed domains are all related to the cyclic hexamers shown in Figure 3a with regard to molecular orientations and intermolecular distances.

To activate deprotonation as a prerequisite for the formation of metal-coordination bonds, samples were first annealed at 100 °C. The subsequently acquired STM image in Figure 1d shows the emergence of new cyclic triangular entities, but also the persistence of the original hexamers with unchanged dimensions. Occasionally, straight interlinked dimers were also observed (examples marked by green arrows) with a center-to-center distance of (1.55 ± 0.08) nm. According to DFT calculations, the targeted bis(diimino)-Cu motif would result in a notably smaller center-to-center distance of 1.29 nm. However, a perfect match is obtained with a dimer, where molecules coordinate two copper atoms linearly arranged on the axis, resulting in a center-to-center distance of 1.54 nm (cf. Supporting Information). The emergence of these new aggregates is also reflected in the XP spectra shown in Figures 2e and f: N 1s is now split into two chemically shifted species, one at the original BE with a relative peak area of 34% and a new majority component at a lower BE of 398.1 eV with a relative peak area of 66%. The lower N 1s BE is characteristic

Accepted Manuscript

This article is protected by copyright. All rights reserved.

for singly deprotonated amino groups in metal-coordination bonds.[14a, 18-19, 24] Distinct changes are similarly observed in C 1s, where the previously observed prominent high BE shoulder appears less pronounced. A satisfying fit is obtained with three components, corresponding to unsubstituted carbons in the triphenylene backbone (C-C: 66%) and two different types of substituted carbons, either binding to fully protonated (C-NH_2: 11%) or singly deprotonated and metal-coordinated (C-NH-Cu: 22%) amino groups. The ratio between the latter two is consistent with the deprotonation ratio deduced from N 1s. Furthermore, C 1s exhibits a slight integral shift to a lower BE of 284.5 eV for the main triphenylene peak.

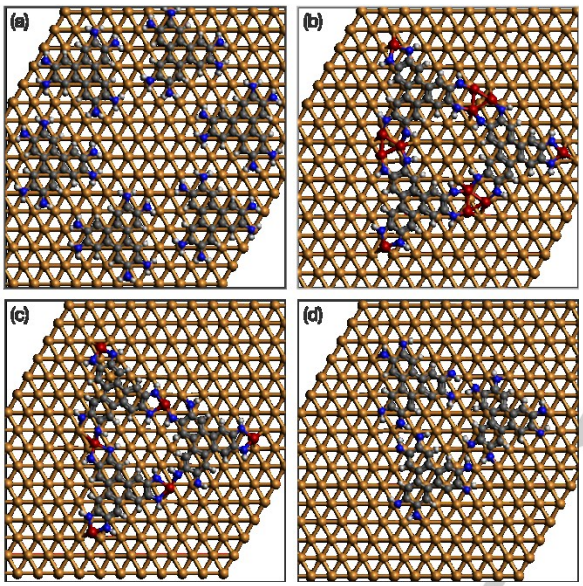

Figure 3. DFT-optimized geometries of HATP structures on Cu(111): a) van-der-Waals bonded hexamer of fully protonated HATP; b) metal-coordinated trimer with Cu_3 coordination centers; c) metal-coordinated trimer with single Cu atom coordination centers; d) imine based hydrogen bonded trimer. (only the topmost copper layer is shown, Cu adatoms are depicted in red)

Annealing to 200 °C triggers progressive deprotonation and formation of metal-coordinated structures. As shown in Figures 2h and i, the chemical changes in XPS previously observed after annealing at 100 °C are driven to completion: N 1s indicates full deprotonation, with only one main peak remaining at a lower BE of 398.1 eV. Accordingly, C 1s again consists of two components, corresponding to carbons in the triphenylene core and carbons substituted with metal-coordinated amino groups, respectively. The deduced peak area ratio of 68:32 again reflects the HATP stoichiometry. The integral peak shift of C 1s to lower BEs is continued with a BE of 284.3 eV, suggesting a correlation with the amount of metal-coordination sites on the molecules.[19] The total intensities of both N 1s and C 1s did not change notably during heating, indicating the absence of molecular desorption. The chemical changes observed in XPS are also accompanied by structural changes as illustrated in the STM image in Figure 1e. Hexamers cannot be discerned anymore; instead, a large variety of different aggregates are observed, with a triangular supramolecular HATP trimer as the common basic unit. These trimers are interlinked into various configurations: (1) head-to-head; (2) cyclic rings consisting of four, five, or six trimers; in addition, individual HATP molecules can be identified attached at the periphery of larger aggregates either as interlink or termination, respective examples are marked by red arrows in Figure 1e and f.

For understanding the structural changes, it is pivotal to resolve the nature of the intermolecular interactions in the trimer. The threefold-symmetry in STM indicates equivalent orientations of all molecules in a trimer, whereas XPS suggests chemical equivalency and deprotonation of all amino groups. Based on this information, DFT simulations were carried out for two metal-coordinated models: either with single Cu atoms or Cu_3 clusters as coordination centers. Alternatively, an imine based hydrogen bonded trimer was considered. The DFT optimized structures of these trimer models on Cu(111) are presented in Figures 3b - d, with intermolecular distances of 1.31 nm, 1.34 nm, and 1.20 nm, for the Cu_3-, Cu-, and hydrogen bonded trimer, respectively. All of these intermolecular distances are consistent with the experimental value of (1.28 ± 0.03) nm within the experimental error. Yet, the best agreement is achieved with the Cu_3 coordination centers that were similarly proposed for tetrahydroxy benzene on Cu(111).[25] Additional support for the Cu_3 coordination centers comes from the XPS data: N 1s indicates a single chemical nitrogen species, whereas the trimer with single Cu atom coordination features nitrogen atoms in inequivalent chemical environments. This argument similarly applies to the hydrogen bonded trimer that contains two types of nitrogen species: hydrogen-bonded and free imine nitrogen atoms. In addition, the literature consistently reports copper-coordination of deprotonated amino groups on copper surfaces,[11, 14a, 19] rendering the formation of this hydrogen bonded structure improbable. From the DFT calculations HATP adsorptions heights of (2.64 ± 0.15) Å and (2.57 ± 0.28) Å were deduced for the Cu_3 and single Cu atom coordinated trimers presented in Figures 3b and c, respectively. These adsorption heights are approximately 0.3 Å lower than those of the van-der-Waals bonded hexamers shown in Figure 3a. The closer proximity to the surface arises from bonding to Cu adatoms (which themselves reside (1.94 … 2.03) Å above the surface). This pulls the coordinating N atoms and also the nearby C atoms closer to the Cu(111) surface (as close as 1.91 Å for the lowest N atom of the single Cu atom-coordinated trimer). Consequently, the C atoms of the central part of the molecules also adsorb closer to the surface than in the van-der-Waals bonded hexamer.

It is worth noting that N 1s XPS indicates deprotonation and copper coordination of all amino groups after annealing to 200 °C. Accordingly, in the DFT calculations copper coordination was also introduced at the peripheral amino groups of the metal-coordinated trimers. This peripheral group coordination could explain the formation of larger aggregates and networks. The STM images in Figures 1e and f reveal the Cu_3-coordinated trimer as the predominating basic motif of the various observed

Accepted Manuscript

This article is protected by copyright. All rights reserved.

aggregates. Prevalence of this supramolecular building unit also indicates a hierarchy of bond strengths, where the intra-trimer bonds are stronger than the inter-trimer bonds. Among the various aggregates head-to-head linked trimers with a pronounced offset along their bond axis account for the majority of aggregates, respective examples are highlighted in Figure 1f. To further elucidate these inter-trimer linkages, DFT simulations were performed, probing metal-coordination linkages comprised of one, two, and three copper atoms. Notably, only linking of the trimers by three copper atoms could reproduce the kinked geometry, also perfectly matching the experimental structure (cf. insert to Figure 1f), whereas linking by either one or two copper atoms results in straight geometries (cf. Supporting Information). Moreover, the postulated hierarchy of bond strengths is underpinned by DFT simulations: For a metal-coordination motif corresponding to the kinked inter-trimer linkage with three Cu atoms a binding energy of 8.52 eV was found, whereas a single Cu_3-coordination motif corresponding to the intra-trimer linkage exhibits a notably higher binding energy of 9.82 eV (cf. Supporting Information).

Additional experiments with three-fold reduced heating rates (0.50 °C min^{-1} instead of 1.66 °C min^{-1}) did not increase the network quality (cf. Supporting Information). Neither did further annealing to 300 °C, where both STM and XPS studies consistently indicate molecular degradation: both a low BE organometallic shoulder at C 1s and the diminished intensity of N 1s suggest dissociation of amino groups (cf. Supporting Information).

HATP on Cu(111) + Ni

To achieve the formation of honeycomb networks based on the four-fold planar bis(diimino)-metal linkages, further experiments were conducted with additional Ni atoms on the surface. First, HATP was deposited onto Cu(111) held at room temperature, followed by co-deposition of Ni. The subsequently acquired STM image in Figure 4a unveils interlinking of molecules into hexagonal porous structures that resemble the targeted honeycomb network. Chemical changes are also corroborated by XPS shown in Figure 5: direct comparison of N 1s and C 1s spectra before and after Ni co-deposition clearly confirms a chemical change in HATP. Both the appearance of a new N 1s component at lower BE and weakening of the high BE shoulder of C 1s consistently indicate a similar kind of transformation as that observed for Cu-coordinated HATP in Figure 2. Fitting of the N 1s spectra suggests a Ni-induced deprotonation of ~50 % of the amino groups. These also give rise to a third component in C 1s, similar to the thermally activated deprotonation on pristine Cu(111). A good fit is achieved by applying the deprotonation ratio obtained from N 1s as a constraint for the relative ratios of the C 1s components. These striking differences to the van-der-Waals bonded structures observed on pristine Cu(111) after room temperature deposition can evidently be attributed to the presence of Ni, whereby the changes in both N 1s and C 1s XPS are analogous to the thermally activated deprotonation on pristine Cu(111). To avoid artefacts known for high molecular coverages due to steric crowding and to ensure full accessibility of all amino groups by Ni adatoms, low molecular coverages were deliberately used for these experiments. This dilution comes at the cost of an inferior signal-to-noise ratio in the XP spectra, in particular for N 1s. Nevertheless, the progressive deprotonation can still unambiguously be verified, in particular when comparing the initial fully protonated state with the final completely deprotonated state in Figures 5a and h. Moreover, the initial deprotonation upon co-deposition of Ni and subsequent thermally-induced further deprotonation is also reflected in the corresponding C 1s data presented in Figure 5 through the weakening of the high BE shoulder. These XPS signatures of the Ni-induced deprotonation are fully consistent with the deprotonation observed on pristine Cu(111).

To activate further deprotonation and network formation, the samples were subsequently annealed to 100 °C. XPS confirms the progressive deprotonation of now approximately 72% of the amino groups directly in N 1s, and indirectly, but consistently also in C 1s by both an increase of the metal-organic component and as an integral peak shift to a lower BE of 284.4 eV. The not yet complete deprotonation is also reflected in STM by the occasional observation of van-der-Waals bonded aggregates similar to those observed at room temperature in the absence of Ni (cf. Figure 1b). One example for such a cyclic structure is marked in Figure 4b. Even though expression of the Ni-coordinated motif is evident this STM image, it does not show complete pores or networks. To drive deprotonation to completion, a second annealing step to 200 °C was performed, resulting in full deprotonation as confirmed by the N 1s and also consistently in the C 1s XP spectra presented in Figures 5h and i: N 1s consist of a single peak at lower BE and C 1s shows full development of the metal-organic component up to the stoichiometric ratio of 33:67 with a constant amount of carbon. An analogous experiment with the five-fold amount of co-deposited Ni similarly resulted only in partial deprotonation at room temperature, whereas full deprotonation still required additional annealing (cf. Supporting Information).

Accepted Manuscript

This article is protected by copyright. All rights reserved.

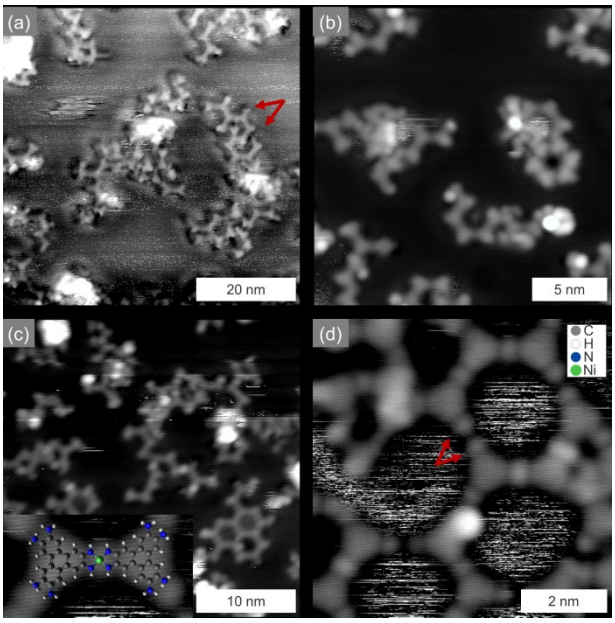

Figure 4. STM images acquired after deposition of HATP and Ni onto Cu(111) at a) room temperature, and after annealing to b) 100 °C, and c) / d) 200 °C; the red arrows highlight terminating Ni atoms; the yellow dashed circle indicates a van-der-Waals bonded cyclic structure (tunneling parameters: a) 0.90 V, 87 pA; b) 0.95 V, 92 pA; c) 3.27 V, 91 pA; d) 0.88 V, 93 pA)

The STM image in Figure 4c now shows network patches consisting of up to three hexagonal metal-coordinated pores, but incomplete pores were still frequently observed. The insert with an overlaid dimer in Figure 4c and the high resolution image in Figure 4d clearly confirm formation of the expected bis(diimino)-Ni binding motif with head-to-head oriented molecules interlinked by a straight metal-coordination bond. Also the experimental center-to-center distance of (1.45 ± 0.1) nm is in accord with the DFT-derived value obtained for a Ni-coordinated hexamer in the gas phase (cf. Supporting Information). Furthermore, a clear signature of the Ni coordination center can now be discerned in the STM contrast as opposed to Cu coordination centers that are often invisible to the STM.[12a, 14, 26] Despite the possibility to form a similar bis(diimino)-Cu motif with intrinsic adatoms of the Cu(111) surface, the Ni motif is strongly preferred, presumably on energetic grounds: the binding energy in the bis(diimino)-Ni coordinated dimer with respect to isolated constituents is calculated to be 9.7 eV, while in the Cu-coordinated dimer it is only 6.0 eV (cf. Supporting Information). Interestingly, the termini of the incomplete pores show bright protrusions, indicating saturation with Ni atoms at the periphery (examples are marked by red arrows in Figure 4d). While further annealing to 260 °C did not improve the network quality, annealing at 300 °C resulted in disordered structures in STM, while XPS indicated molecular decomposition (cf. Supporting Information).

Additional DFT simulations were performed aiming at elucidating the role of epitaxial effects of the Cu(111) surface for the Ni-coordinated structures (cf. Supporting Information). In the first step, a cyclic Ni-coordinated hexamer was optimized in the gas phase, resulting in a distance of 1.27 nm between directly linked HATP molecules. This intermolecular distance closely corresponds to 5-times the Cu(111) lattice parameter (1.28 nm), hence this size and symmetry match between the Ni-coordinated honeycomb network and the Cu(111) surface should foster a nearly perfect epitaxial relation. Indeed, DFT simulations with periodic boundary conditions of a fully reticulated Ni-coordinated honeycomb network adsorbed on Cu(111) corroborate a perfect match, whereby the two non-equivalent molecules within the unit cell can adsorb with their preferred geometry (i.e. with the centres of aromatic rings above fcc sites, cf. Supporting Information). Accordingly, surface registry effects are unlikely to account for the absence of extended Ni-coordinated honeycomb networks on Cu(111).

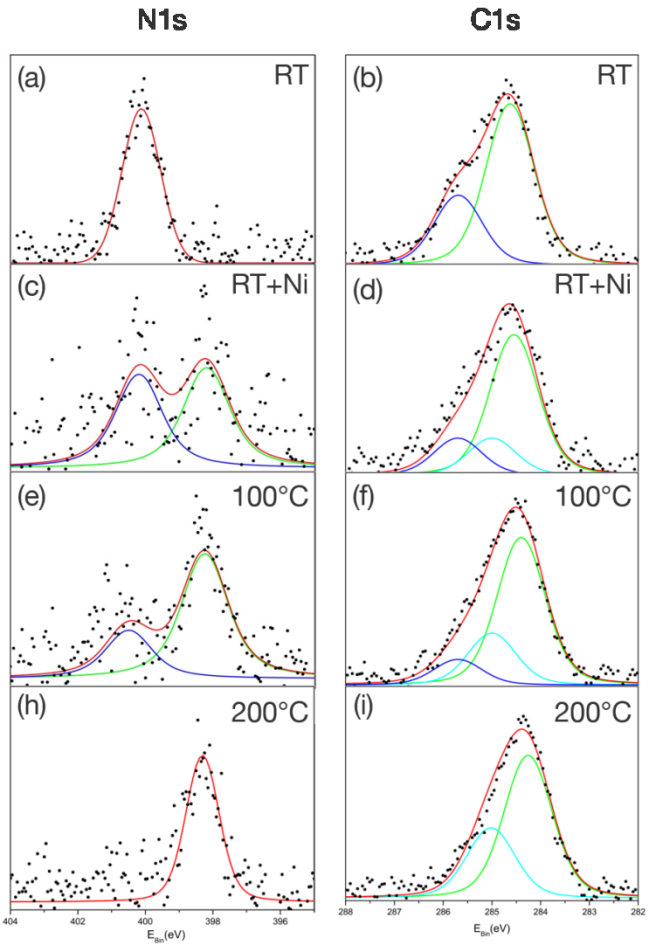

Figure 5. XP spectra of N 1s and C 1s core levels acquired after a) / b) room temperature deposition of HATP on Cu(111), c) / d), after additional deposition of Ni, and annealing to e) / f) 100 °C, and h) / i) 200 °C. Data is represented by black dots; red lines correspond to the sum of all fitted components; N 1s and C 1s components are assigned to the following colour scheme: NH_2 (green), NH-Ni (blue), C-C (green), C-NH_2 (blue), C-NH-Ni (light blue).

To achieve the growth of extended and highly regular metal-coordination networks, the ratio of molecules to coordination centers is a further, potentially decisive parameter.[27] Therefore,

Accepted Manuscript

This article is protected by copyright. All rights reserved.

additional experiments were carried out with lower (~30%) and higher (~4-fold) amounts of Ni, while the amount of molecules was kept constant. Similarly, HATP was deposited first onto Cu(111) held at room temperature, then Ni was co-deposited in the three different coverages, and finally, the samples were annealed to 200 °C. The STM image for "low" Ni coverage in Figure 6a shows two co-existing different metal-coordination motifs: the trimer based structures as observed on pristine Cu(111) and the straight motifs as observed in the presence of Ni. This indicates that the amount of Ni was too small to suppress Cu coordination. For the previously applied Ni coverage the results are consistent, exclusively showing the bis(diimino)-Ni motif. At "high" Ni coverage the onset of cluster formation on the surface can be seen in Figure 6c. Although exclusively the Ni coordination motif is observed, the size of metal-organic networks is markedly diminished.

.

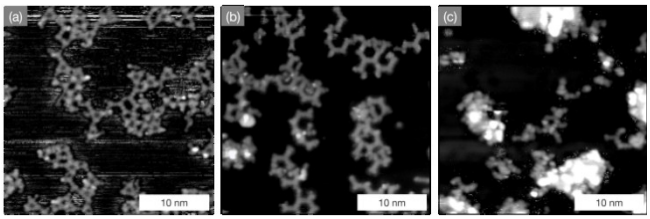

Figure 6. STM images of HATP on Cu(111) acquired after deposition of different amounts of Ni and subsequent annealing to 200 °C; a) "low" Ni coverage (30%); b) previously applied Ni coverage (100%); c) "high" Ni coverage (400%) (tunneling parameters: a) 0.88 V, 55 pA; b) 1.80 V, 100 pA; c) 3.20 V, 89 pA).

Conclusions

The observed structural and chemical changes of HATP on pristine and Ni-covered Cu(111) surfaces are summarized in Figure 7. HATP molecules remained chemically unaltered upon room temperature deposition onto pristine Cu(111). The absence of deprotonation of amino-functionalized compounds under these conditions is common,[11, 14a, 22] whereas on more reactive Ni(111) surfaces partial deprotonation can readily occur.[17a, 18] Despite the fact that HATP molecules are not equipped for strong intermolecular bonds, stable self-assemblies could be imaged by STM at room temperature. Since intermolecular metal-coordination and hydrogen bonds were ruled out, the cohesion of these aggregates must solely arise from van-der-Waals interactions. According to DFT calculations, the intermolecular binding energies are extremely small, but a strong and highly site-specific adsorption of the triphenylene core on Cu(111) largely accounts for the stabilization. Subsequent annealing triggered the well-known thermally activated deprotonation on pristine Cu(111).[11, 14a, 22] This provided the basic prerequisite for formation of metal-coordination bonds, unexpectedly with Cu_3 clusters as coordination centers. Albeit single atom coordination motifs are most common on surfaces, a similar Cu_3 motif was previously proposed for tetrahydroxy benzene on Cu(111).[25] In this respect, it appears more surprising that the expected bis(diimino)-Cu motif was not observed on Cu(111), given its predominance at liquid interfaces.[5] This hints towards thermodynamic preference for the copper-rich Cu_3 coordination on Cu(111). Notwithstanding that this motif would in principle allow the extension into fully reticulated and regular 2D networks, only various aggregates comprised of interlinked supramolecular trimers were observed. The experimentally observed kinked structure of two connected supramolecular trimers was reproduced by DFT simulations with three coordinating copper atoms in the interlink. According to DFT calculations, the inter-trimer linkages have a smaller binding energy than the intra-trimer linkages. This hierarchy of bond strengths can explain the hierarchical structure formation based on a stable supramolecular Cu_3-coordinated trimer as secondary building unit. A possible explanation for the absence of extended networks on pristine Cu(111) is offered by pronounced adsorption site preferences of both the triphenylene backbones and the Cu_3 clusters that cannot be met both at the same time in larger networks.

Co-deposition of the more reactive Ni triggers deprotonation already at room temperature, clearly indicating adatom mediated surface chemistry. However, full deprotonation at room temperature was not achieved, even when significantly higher amounts of Ni were deposited. In the competition with metal-coordination by Cu adatoms, a distinct preference for Ni-coordination is expressed. Accordingly, insufficient amounts of Ni can be held responsible for the observed co-existence of Ni-coordination and Cu-coordination. Here we found 50% deprotonation after co-deposition of Ni at room temperature, whereas the thermally induced further deprotonation showed a temperature progression comparable to pristine Cu(111). This suggests that the thermally driven process is Cu-driven without any further notable contributions from Ni. Even though small patches of the targeted honeycomb network were formed, extended regular structures remained elusive. DFT simulations suggest that a fully reticulated Ni-coordinated honeycomb network can be commensurate with the Cu(111) surface, whereby the two non-equivalent molecules of the unit cell adopt their preferred adsorption geometry. Consequently, these simulations indicate that a lattice mismatch cannot be held responsible for the absence of extended Ni-coordinated honeycomb networks on Cu(111). Yet, the experiments with variable amounts of co-deposited Ni indicate a limited bond reversibility of the strong Ni coordination bonds. This prevents the fusion of the smaller fragments, hence decisively hampers the growth of extended networks. This is further underpinned by DFT, suggesting a more than 50% higher binding energy for Ni- than for Cu-coordination, i.e. 9.7 eV vs. 6.0 eV for the isolated dimer. The diminished size of molecular aggregates observed for larger amounts of Ni provides further experimental evidence for this hypothesis. This restricted bond reversibility is a decisive difference compared to the situation at liquid interfaces, where extended self-supporting networks can be obtained.[3d] Consequently, the aqueous subphase must play a vitally important role for the reversibility of the metal-organic coordination bonds. Higher temperatures, that could in principle

Accepted Manuscript

This article is protected by copyright. All rights reserved.

induce bond reversibility also on Cu(111), are prohibitive, as this leads to molecular decomposition, presumably by dissociation of the amino groups.

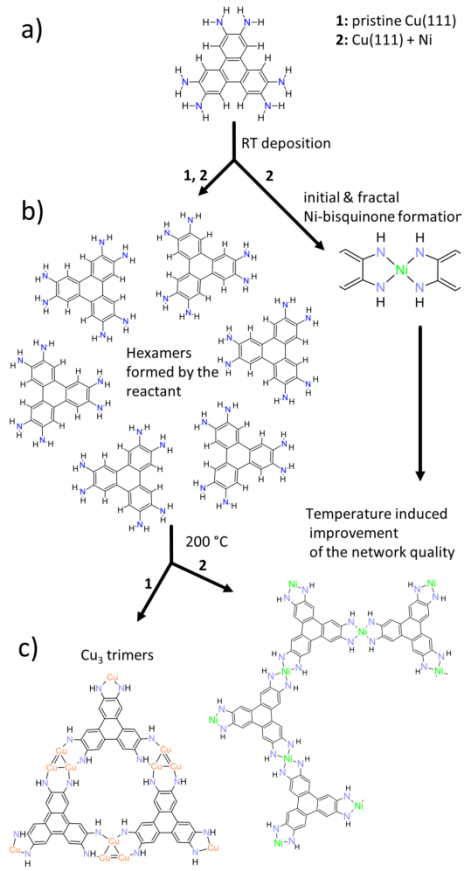

Figure 7. Summary of thermally and Ni-induced structural and chemical changes of HATP on pristine and Ni-covered Cu(111)

In summary, studying the formation of metal-coordinated networks from HATP on Cu(111) under UHV conditions substantially benefits from the possibility of acquiring high-resolution STM images and complementary chemical information from XPS. Important differences to the synthesis at liquid interfaces become apparent: (1) the high availability of adatoms as coordination centers on solid metal surfaces promotes the expression of multi-atomic coordination motifs; (2) distinct adsorption-site preferences impose further constraints on crystalline surfaces that may hamper the formation of extended networks in the present case; (3) the absence of the liquid subphase substantially affects metal-organic bond formation, with possible consequences for bond reversibility.

Materials and Methods

STM and XPS experiments were carried out under UHV conditions at base pressures below 3×10^{-10} mbar. For STM (XPS) experiments Cu(111) single crystals were prepared by cycles of 0.5 (1.0) keV Ar^+-ion sputtering and radiative (e-beam) annealing at 500 °C. HATP (cf. Supporting Information for synthesis) was deposited by sublimation from a home-built Knudsen-cell[28] with a crucible temperature of 225 °C at a pressure of 3×10^{-9} mbar. Nickel (0.5 mm diameter wire, 99.99%, MaTecK) was deposited from an Omicron EFM 3 e-beam evaporator using a molybdenum crucible and deposition rates were controlled with the internal flux monitor. For all sample annealing steps a standard heating and cooling rate of 1.66 °C min^{-1} was applied, if not noted otherwise.

STM data were acquired *in-situ* at room temperature with a home-built instrument controlled by an SPM100 controller (RHK Technology Inc.). XPS measurements were carried out in a SPECS system equipped with a monochromatic XR50M X-ray source and Phoibos 150 electron analyzer. XP spectra were acquired using a Al-K_α source with a photon energy of 1486.3 eV at normal electron emission with a pass energy of 20 eV. For energy calibration a Cu $3p_{3/2}$ binding energy of 70.1 eV was used as internal standard.[29] XP spectra were fitted by Voigt-functions after subtraction of linear backgrounds. For a given element similar peak widths were applied for all chemically shifted components.

DFT simulations were carried out with the CP2K software.[30] The PBE functional was employed[31] with the D3 dispersion correction,[32] Goedecker-Teter-Hutter pseudopotentials,[33] and double-zeta valence polarized basis sets.[34] The Brillouin zone was sampled only at the Γ point. Isolated aggregates were modelled as non-periodic systems; their z-coordinates (vertical) were fixed to maintain planarity to mimic the presence of a surface. Calculations of adsorbates on the Cu(111) surface were performed using periodic boundary conditions, i.e. the Cu(111) slabs (and all slab-adsorbate systems) were periodic in two dimensions; along the z direction the slabs were separated by 10 Å vacuum. Two-layer thick slabs were used, with atomic positions in the bottom layer fixed, while the top layer and all adsorbates were allowed to relax. 16×16-expanded Cu(111) slabs were used for the van-der-Waals bonded hexamers and the supramolecular trimers. This lateral size of the slabs guaranteed a minimum spacing of 6 Å between the periodic repetitions of the molecular aggregates, i.e. large enough to exclude interactions between neighbouring hexamers and trimers in image cells; 15×15-expanded Cu(111) slabs were used for the Ni-coordinated honeycomb networks, resulting in a fully reticulated commensurate $5\sqrt{3} \times 5\sqrt{3}$ R30° superstructure. All structure files can be downloaded from: https://figshare.com/s/e5573906428dfbf16dfa

Acknowledgements

The excellence cluster Nanosystems Initiative Munich is gratefully acknowledged for financial support. The Authors thank Karl Eberle for support and technical assistance during XPS measurements. N.M. acknowledges the use of Iceberg and ShARC high-performance computing clusters at the University of Sheffield and the use of the THOMAS high-performance cluster which is partially funded by EPSRC (EP/P020194) and was accessed via our membership of the UK's HEC Materials Chemistry Consortium (funded by EPSRC EP/L000202).

Keywords: metal-coordination • hexaaminotriphenylene • Cu(111) • Scanning Tunneling Microscopy • X-ray Photoelectron Spectroscopy

Accepted Manuscript

This article is protected by copyright. All rights reserved.

[1] a) J. Sakamoto, J. van Heijst, O. Lukin, A. D. Schlüter, *Angew. Chem., Int. Ed.* **2009**, *48*, 1030-1069; b) D. F. Perepichka, F. Rosei, *Science* **2009**, *323*, 216-217; c) J. V. Barth, *Annu. Rev. Phys. Chem.* **2007**, *58*, 375-407.

[2] a) R. Sakamoto, K. Takada, X. Sun, T. Pal, T. Tsukamoto, E. J. H. Phua, A. Rapakousiou, K. Hoshiko, H. Nishihara, *Coord. Chem. Rev.* **2016**, *320-321*, 118-128; b) R. Sakamoto, K. Takada, T. Pal, H. Maeda, T. Kambe, H. Nishihara, *Chem. Commun.* **2017**, *53*, 5781-5801; c) T. Bauer, Z. Zheng, A. Renn, R. Enning, A. Stemmer, J. Sakamoto, A. D. Schlüter, *Angew. Chem. Int. Ed.* **2011**, *50*, 7879-7884; d) L. Chen, J. Kim, T. Ishizuka, Y. Honsho, A. Saeki, S. Seki, H. Ihee, D. Jiang, *J. Am. Chem. Soc.* **2009**, *131*, 7287-7292.

[3] a) R. Dong, Z. Zheng, D. Tranca, J. Zhang, N. Chandrasekhar, S. Liu, X. Zhuang, G. Seifert, X. Feng, *Chem. Eur. J.* **2016**, *23*, 2255–2260; b) R. Dong, M. Pfeffermann, H. Liang, Z. Zheng, X. Zhu, J. Zhang, X. Feng, *Angew. Chem. Int. Ed.* **2015**, *54*, 12058-12063; c) D. Sheberla, J. C. Bachman, J. S. Elias, C.-J. Sun, Y. Shao-Horn, M. Dincă, *Nat. Mat.* **2016**, *16*, 220-224; d) D. Sheberla, L. Sun, M. A. Blood-Forsythe, S. Er, C. R. Wade, C. K. Brozek, A. n. Aspuru-Guzik, M. Dincă, *J. Am. Chem. Soc.* **2014**, *136*, 8859-8862; e) L. Giovanelli, O. Ourdjini, M. Abel, R. Pawlak, J. Fujii, L. Porte, J.-M. Themlin, S. Clair, *J. Phys. Chem. C* **2014**, *118*, 14899-14904; f) R. Coratger, B. Calmettes, M. Abel, L. Porte, *Surf. Sci.* **2011**, *605*, 831-837.

[4] D. Herebian, E. Bothe, F. Neese, T. Weyhermüller, K. Wieghardt, *J. Am. Chem. Soc.* **2003**, *125*, 9116-9128.

[5] M. G. Campbell, D. Sheberla, S. F. Liu, T. M. Swager, M. Dincă, *Angew. Chem., Int. Ed.* **2015**, *54*, 4349-4352.

[6] E. M. Miner, T. Fukushima, D. Sheberla, L. Sun, Y. Surendranath, M. Dincă, *Nat. Commun.* **2016**, *7*, 10942.

[7] C. Yang, K. S. Schellhammer, F. Ortmann, S. Sun, R. Dong, M. Karakus, Z. Mics, M. Löffler, F. Zhang, X. Zhuang, E. Cánovas, G. Cuniberti, M. Bonn, X. Feng, *Angew. Chem. Int. Ed.* **2017**, *56* 3920-3924.

[8] X. Huang, S. Zhang, L. Liu, L. Yu, G. Chen, W. Xu, D. Zhu, *Angew. Chem. Int. Ed.* **2017**, *57*, 146-150.

[9] D. J. Murray, D. D. Patterson, P. Payamyar, R. Bhola, W. Song, M. Lackinger, A. D. Schlüter, B. T. King, *J. Am. Chem. Soc.* **2015**, *137*, 3450-3453.

[10] a) N. A. A. Zwaneveld, R. Pawlak, M. Abel, D. Catalin, D. Gigmes, D. Bertin, L. Porte, *J. Am. Chem. Soc.* **2008**, *130*, 6678-6679; b) J. F. Dienstmaier, D. D. Medina, M. Dogru, P. Knochel, T. Bein, W. M. Heckl, M. Lackinger, *ACS Nano* **2012**, *6*, 7234-7242; c) S. Spitzer, A. Rastgoo-Lahrood, K. Macknapp, V. Ritter, S. Sotier, W. M. Heckl, M. Lackinger, *Chem. Commun.* **2017**, *53*, 5147-5150.

[11] M. Knor, H.-Y. Gao, S. Amirjalayer, A. Studer, H. Gao, S. Du, H. Fuchs, *Chem. Commun.* **2015**, *51*, 10854-10857.

[12] a) T. Sirtl, S. Schlögl, A. Rastgoo-Lahrood, J. Jelic, S. Neogi, M. Schmittel, W. M. Heckl, K. Reuter, M. Lackinger, *J. Am. Chem. Soc.* **2013**, *135*, 691-695; b) S. Stepanow, N. Lin, D. Payer, U. Schlickum, F. Klappenberger, G. Zoppellaro, M. Ruben, H. Brune, J. V. Barth, K. Kern, *Angew. Chem., Int. Ed.* **2007**, *119*, 724-727; c) K. Müller, J. C. Moreno-López, S. Gottardi, U. Meinhardt, H. Yildirim, A. Kara, M. Kivala, M. Stöhr, *Chem. Eur. J.* **2015**, *22*, 581-589 ; d) U. Schlickum, R. Decker, F. Klappenberger, G. Zoppellaro, S. Klyatskaya, W. Auwärter, S. Neppl, K. Kern, H. Brune, M. Ruben, J. V. Barth, *J. Am. Chem. Soc.* **2008**, *130*, 11778-11782.

[13] Y. Li, J. Xiao, T. E. Shubina, M. Chen, Z. Shi, M. Schmid, H.-P. Steinrück, J. M. Gottfried, N. Lin, *J. Am. Chem. Soc.* **2012**, *134*, 6401-6408.

[14] a) A. Shchyrba, C. Wäckerlin, J. Nowakowski, S. Nowakowska, J. Björk, S. Fatayer, J. Girovsky, T. Nijs, S. C. Martens, A. Kleibert, M. Stöhr, N. Ballav, T. A. Jung, L. H. Gade, *J. Am. Chem. Soc.* **2014**, *136*, 9355-9363; b) M. Matena, J. Björk, M. Wahl, T.-L. Lee, J. Zegenhagen, L. H. Gade, T. A. Jung, M. Persson, M. Stöhr, *Phys. Rev. B* **2014**, *90*, 125408.

[15] L. Jiang, A. C. Papageorgiou, S. C. Oh, Ö. Sağlam, J. Reichert, D. A. Duncan, Y.-Q. Zhang, F. Klappenberger, Y. Guo, F. Allegretti, S. More, R. Bhosale, A. Mateo-Alonso, J. V. Barth, *ACS Nano* **2016**, *10*, 1033-1041.

[16] L. Dong, Z. A. Gao, N. Lin, *Prog Surf Sci* **2016**, *91*, 101-135.

[17] a) S. X. Huang, D. A. Fischer, J. L. Gland, *J. Phys. Chem.* **1996**, *100*, 10223-10234; b) X. Xu, C. M. Friend, *J. Vac. Sci. Technol* **1991**, *9*, 1599-1603.

[18] T. S. Jones, M. R. Ashton, N. V. Richardson, R. G. Mack, W. N. Unertl, *J. Vac. Sci. Technol* **1990**, *8*, 2370-2375.

[19] Y.-P. Lin, O. Ourdjini, L. Giovanelli, S. Clair, T. Faury, Y. Ksari, J.-M. Themlin, L. Porte, M. Abel, *J. Phys. Chem. C* **2013**, *117*, 9895-9902.

[20] a) J. Hwang, Y. Kim, Y. Ahn, *Bull. Korean Chem. Soc.* **2014**, *35*, 2831-2834; b) J. L. Solomon, R. J. Madix, J. Stöhr, *Surf. Sci.* **1991**, *255*, 12-30.

[21] a) A. C. Papageorgiou, S. Fischer, J. Reichert, K. Diller, F. Blobner, F. Klappenberger, F. Allegretti, A. P. Seitsonen, J. V. Barth, *ACS Nano* **2012**, *6*, 2477-2486; b) K. Diller, F. Klappenberger, M. Marschall, K. Hermann, A. Nefedov, C. Wöll, J. V. Barth, *J. Chem. Phys* **2012**, *136*, 014705; c) T. C. Chiang, G. Kaindl, T. Mandel, *Phys. Rev. B* **1986**, *33*, 695-711; d) S. Kohiki, K. Oki, F. Konishi, *Anal. Sci.* **1985**, *1*, 115-117.

[22] F. Masini, Y. Ning, Z. Li, E. Lægsgaard, F. Besenbacher, T. R. Linderoth, *Chem. Commun.* **2013**, *49*, 8665.

[23] a) W. Liu, V. G. Ruiz, G.-X. Zhang, B. Santra, X. Ren, M. Scheffler, A. Tkatchenko, *New J. Phys.* **2013**, *15*, 053046; b) X.-Q. Shi, Y. Li, M. A. V. Hove, R.-Q. Zhang, *J. Phys. Chem. C* **2012**, *116*, 23603-23607.

[24] P. R. Davies, D. Edwards, D. Richards, *J. Phys. Chem. B* **2004**, *108*, 18630-18639.

[25] F. Bebensee, K. Svane, C. Bombis, F. Masini, S. Klyatskaya, F. Besenbacher, M. Ruben, B. Hammer, T. R. Linderoth, *Angew. Chem. Int. Ed.* **2014**, *53*, 12955-12959.

[26] a) H. Walch, J. Dienstmaier, G. Eder, R. Gutzler, S. Schlögl, T. Sirtl, K. Das, M. Schmittel, M. Lackinger, *J. Am. Chem. Soc.* **2011**, *133*, 7909-7915; b) J. Björk, M. Matena, M. S. Dyer, M. Enache, J. Lobo-Checa, L. H. Gade, T. A. Jung, M. Stöhr, M. Persson, *Phys. Chem. Chem. Phys.* **2010**, *12*, 8815; c) S. L. Tait, A. Langner, N. Lin, S. Stepanow, C. Rajadurai, M. Ruben, K. Kern, *J. Phys. Chem. C* **2007**, *111*, 10982-10987.

[27] a) X. Zhang, G. Gu, N. Li, H. Wang, H. Tang, Y. Zhang, S. Hou, Y. Wang, *RSC Adv.* **2018**, *8*, 1852-1856; b) U. Schlickum, F. Klappenberger, R. Decker, G. Zoppellaro, S. Klyatskaya, M. Ruben, K. Kern, H. Brune, J. V. Barth, *J. Phys. Chem. C* **2010**, *114*, 15602-15606.

[28] R. Gutzler, W. M. Heckl, M. Lackinger, *Rev. Sci. Instrum.* **2010**, *81*, 015108.

[29] N. S. McIntyre, M. G. Cook, *Anal. Chem* **1975**, *47*, 2208-2213.

[30] J. VandeVondele, M. Krack, F. Mohamed, M. Parrinello, T. Chassaing, J. Hutter, *Comput. Phys. Commun.* **2005**, *167*, 103-128.

[31] J. P. Perdew, K. Burke, M. Ernzerhof, *Phys. Rev. Lett.* **1996**, *77*, 3865-3868.

[32] S. Grimme, J. Antony, S. Ehrlich, H. Krieg, *J. Chem. Phys* **2010**, *132*, 154104.

[33] S. Goedecker, M. Teter, J. Hutter, *Phys. Rev. B* **1996**, *54*, 1703-1710.

[34] J. VandeVondele, J. Hutter, *J. Chem. Phys* **2007**, *127*, 114105.

Accepted Manuscript

This article is protected by copyright. All rights reserved.

10.1002/chem.201803908

WILEY-VCH

FULL PAPER

The interplay between self-assembly and surface chemistry of hexaaminotriphenylene was comparatively studied on pristine vs. Ni-covered Cu(111) surfaces. Without Ni, coordination by Cu_3 clusters was observed, whereas in the presence of Ni the bis(diimino)-Ni motif was dominating.

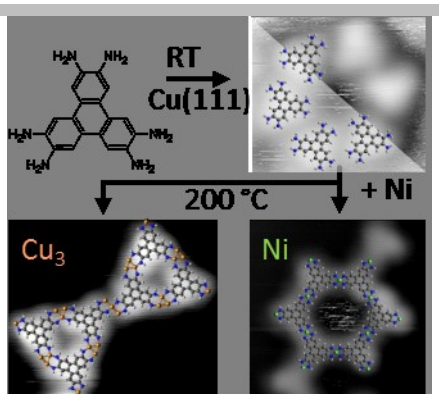

*Matthias Lischka, Renhao Dong, Mingchao Wang, Natalia Martsinovich, Massimo Fritton, Lukas Grossmann, Wolfgang M. Heckl, Xinliang Feng, Markus Lackinger**

Page No.– Page No.

Competitive metal-coordination of hexaaminotriphenylene on Cu(111) by intrinsic copper *versus* extrinsic nickel adatoms

WILEY-VCH

Accepted Manuscript

This article is protected by copyright. All rights reserved.